Ultrasonics - Sonochemistry 41 (2018) 651–660

Contents lists available at ScienceDirect

Ultrasonics - Sonochemistry

journal homepage: www.elsevier.com/locate/ultson

Fabrication of g-C_3N_4/NiO heterostructured nanocomposite modified glassy carbon electrode for quercetin biosensor

S. Selvarajan[a], A. Suganthi[a,b,*], M. Rajarajan[c,*]

[a] PG & Research Department of Chemistry, Thiagarajar College, Madurai 625009, Tamilnadu, India
[b] Mother Teresa Women's University, Kodaikanal 624 102, Tamilnadu, India
[c] Directorate of Distance Education, Madurai Kamaraj University, Madurai 625 021, Tamilnadu, India

ARTICLE INFO

Keywords:
Synthesis
Nanocomposite
Quercetin
Electrocatalytic activity
Real samples

ABSTRACT

Herein, we report a one-pot synthesis of structurally uniform and electrochemically active graphitic carbon nitride/nickel oxide (g-C_3N_4/NiO) nanocomposite and an investigation on the electrocatalytic oxidation of quercetin (QR). The synthesized g-C_3N_4/NiO nanocomposite has uniform surface distribution, which was characterized with scanning electron microscopy (SEM). Moreover, the composition of synthesized g-C_3N_4/NiO nanocomposite was characterized by UV–vis-spectroscopy, X-ray diffraction (XRD), Fourier transform infrared spectroscopy (FT-IR spectra), BET, SEM and HRTEM. The g-C_3N_4/NiO was electrochemically treated in 0.1 MPBS solution through cyclic voltammetry (CV) and differential pulse voltammetry (DPV). The peak current response increases linearly with QR concentration from 0.010 μM to 250 μM with a fast response time of less than 2 s and a detection limit of 0.002 μM. To further evaluate the feasibility of using this sensor for real sample analysis, QR content in various real samples including green tea, green apple, honey suckle were determined and satisfactory results were achieved.

1. Introduction

Flavonoids are natural products widely distributed in the plant kingdom and generally present in the common human diet [1–3]. There is a considerable amount of epidemiological evidences associating rich diets in fresh fruits and vegetables (onions, apples, various berries, tea, etc) to lower risks of suffering from cardiovascular conditions and certain types of cancer [4]. Pharmacological studies have demonstrated that some phenolic compounds possess anti-inflammatory, antiviral and antifungal properties as well as an antiproliferative effect on tumor cells [5]. Several of these biological effects are related to radical scavenging (antioxidant) properties of such compounds [6,7]. Radical reactions occur in many biological processes as a natural consequence of living in an oxidizing environment. However damaging radical reactions outcome when an unusual process takes place. Interesting reports on the role of free radicals and antioxidants were reported by Thomas and Lobo et al. [8,9].

Quercetin (3,3′,4′,5,7-pentahydroxy-flavone, Scheme 1), is a flavonoid of widespread occurrence in nature whose medicinal properties have been extensively demonstrated in the literature, especially the antioxidant capacity [10–13]. The antioxidant properties of these compounds (flavonoids) have been attributed to their capacity to scavenge free radicals generated in aqueous phase, increasing the resistance of lipids against peroxidation. Despite this, the electrochemical behavior of quercetin has been almost always studied in organic solvents due to constrain imposed by its solubility characteristics. Evidently, the stability of intermediate species originated by oxidation reactions is substantially different depending on the surroundings (organic or aqueous media), [14] offering a very rich chemistry as consequence. In this framework, the knowledge of its electrochemical behavior in biological relevant to get insight into the quercetin action as antioxidant.

The most commonly used technique for the determination of QR are high-performance liquid chromatography [15] and capillary electrophoresis [16–19], which have been effectively used for the determination and quantification, coupled with various detection techniques [20], such as UV-spectrophotometry, UV photodiode array detection, mass spectrometry, electrochemical detection and chemiluminescence. The above methods may provide high assay selectivity, but also leads to some disadvantages such as operational complexity, time and reagent consumption, high cost, etc. In fact, some direct methods for analysis of quercetin without pre-separation have also been described. They are mostly based on chemical derivatization combined with UV spectrophotometry [21], or a Kalman filter approach [22,23], but have a poor

* Corresponding authors at: PG & Research Department of Chemistry, Thiagarajar College, Madurai 625009, Tamilnadu, India (A. Suganthi).
E-mail addresses: suganthiphd09@gmail.com (A. Suganthi), rajarajan_1962@yahoo.com (M. Rajarajan).

http://dx.doi.org/10.1016/j.ultsonch.2017.10.032
Received 12 September 2017; Received in revised form 29 October 2017; Accepted 30 October 2017
Available online 01 November 2017
1350-4177/

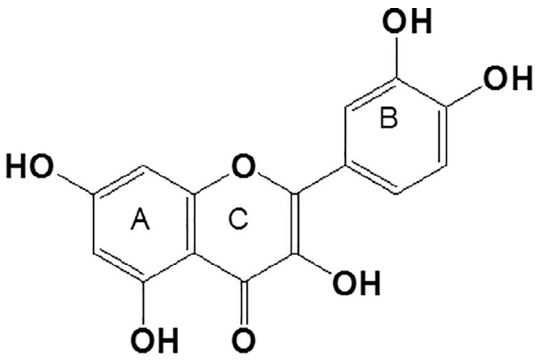

Scheme 1. Chemical structure of quercetin molecule.

detection limit. Because quercetin is electrochemically active, electrochemical methods with their advantages of higher sensitivity, low cost and less interferences from non-electroactive substances are preferable. The electrochemical oxidation of QR was studied by Masek et al. [24,25], under different conditions. In recent years, significant emphasis has been placed on the development of electrochemical sensor for QR detection [26–29].

Usage of ultrasonic irradiation is a simple, green, and low-cost route for the preparation blend nanocomposites (NCs). With the usage of ultrasonic, extra-ordinary reaction conditions like activation surface, high pressure, and high temperature are created for a very short time in a liquid that cannot be achieved by other methods such as mechanical or magnetic stirring. These reaction conditions are created by cavitation micro-bubbles (formation, growth, and collapse of microbubbles in a liquid). With collapsing of microbubbles, the concentrated energy stored in the microbubbles release within a very short time (with a heating and cooling rate of $> 1010\,K\,s^{-1}$). Furthermore, this route provides an excellent homogeneous blend NC with a good dispersion and distribution that is necessary to obtain a good blend NC with improved properties. The results showed that thermal stability, morphology, and optical property were improved in comparison with the pure blend [30–32]. Inorganic nanomaterials, such as Cu, Fe, Ni, and their oxides and sulfides, have attracted considerable attention as sensors and biosensors due to their low cost, high specific surface area, good electrocatalytic activity, and the possibility of promoting electron transfer rates. Recently, some forms of Ni and NiO nanomaterials have been utilized in the fabrication of biosensors because they are inexpensive, nontoxic and due to their readily stored properties [33,34].

g-C_3N_4, a two-dimensional (2D) planar conjugation material, unique electronic band structure, has large surface area, high thermal, chemical stability, and catalytic properties. Similar to graphite, g-C_3N_4 has a layered structure involving weak van der Waals interaction between the adjacent C—N layers. Therefore, inspired by the research of graphene, much work has been conducted for the achievement of g-C_3N_4 nanosheet and the ultrathin g-C_3N_4 nanosheets are excellent performance for photocatalysis or bisosensing [35–37]. Some carbon based nanocomposites have been used to supercapacitive [38,39], catalysis [40,41], photoelectrochemical [42], hydrogen production [43] and sensor [44,45], respectively. The homogeneous nanoparticles are undesirable for biological and pharmaceutical applications because of their number of drawbacks, such as easy aggregation or precipitation, less electron transfer properties, and less electrocatalytic stability and recycling.

To tackle these problems, synthesis of g-C_3N_4 composites with different nanomaterials is a common preferred way. But again the main drawback associated with homogenous nanomaterials is poor stability and selectivity during sensing process. Hence it is imperative to design and develop a nanocomposite with high surface area, long-term stability, high electrocatalytic activity, and reusability, which should be able to promote the kinetics of electron transfer reactions. These features are able to be achieved only by binary nanocomposite materials, such as the one proposed in this article. To the best of our knowledge, there is no report on the sonochemical synthesis of g-C_3N_4/NiO nanocomposite as an electrochemical sensor. Therefore, it would be of great significance and innovation to broaden the application of the g-C_3N_4/NiO composites in the electrochemical sensor.

Here, the desired electrode was sonochemical synthesis and fabricated simply by growing prickly g-C_3N_4/NiO nanocomposite directly on electrode substrates via a drop casting method and without using any organic reagent. The modified electrode was discovered to have strong electrocatalytic activity toward QR, with a concurrent lowering of the QR oxidation potential. The influence of the modified electrode on several parameters, including pH, scan rate, concentration, as well as interference substances, was also studied.

2. Experimental section

2.1. Materials

All reagents and chemicals used in this study were analytical grade and purchased from Merck and used as received without further purification. All solutions were prepared with deionized water.

2.2. Synthesis of g-C_3N_4

The bulk g-C_3N_4 was synthesized by direct thermal polycondensation of melamine according to previous report [46]. Graphitic carbon nitride (g-C_3N_4) powder was prepared by directly heating melamine at 550 °C in a muffle furnace for 4 h with a heating rate of 10 °C min^{-1} under air condition. The product was washed with ethanol and deionized water several times, and collected by centrifugation and finally dried at 60 °C in air.

2.3. Synthesis of g-C_3N_4/NiO nanocomposite

10 mg of g-C_3N_4 was dispersed in 50 ml DD water followed by ultrasonication (300 W) for 2 h while the 5 mM of $NiCl_2{\cdot}6H_2O$ was dissolved in 10 ml DD water. After mixing these two solutions with 30 min of vigorous agitation, 0.1 M NaOH solution was introduced drop wise into the mixture to adjust the pH to 11. Then, the solution was heated at 50 °C for 30 min with stirring and sonication (300 W), followed by refluxing for 8 h. At last, green precipitate was obtained and rinsed with ethanol and deionized water several times. The resulting nanocomposites were dried at 60 °C for 24 h, until the decomposition of volatile compounds hydrated minerals and unwanted ions. After annealing at 300 °C for 1 h in air, the g-C_3N_4/NiO nanocomposite was obtained (1:5 ratio). For the synthesis of pure NiO, the conditions are identical, except for the absence of g-C_3N_4 in the system [47]. The overall experimental synthesis mechanisms are clearly documented in Scheme 2.

2.4. Fabrication of g-C_3N_4/NiO nanocomposite modified GCE

Prior to use, GCE (diameter = 3 mm) was carefully polished to a mirror like plane with 0.5 and 0.05 μm alumina slurries, then cleaned ultrasonically in water and acetone, successively. Afterwards, the electrode was washed thoroughly with excess amounts of water and dried under nitrogen gas. Schematic diagram showing the step-wise fabrication of g-C_3N_4/NiO/GCE is shown in Scheme 2. 4μL of 3.1 mg/mL g-C_3N_4/NiO colloid suspension was dropped onto the pretreated GCE and allowed to dry under ambient condition for 3 h to obtain the g-C_3N_4/NiO modified GCE. Then, the electrode was rinsed thoroughly with deionized water to remove the physically adsorbed materials to form the g-C_3N_4/NiO_2electrode for QR sensing.

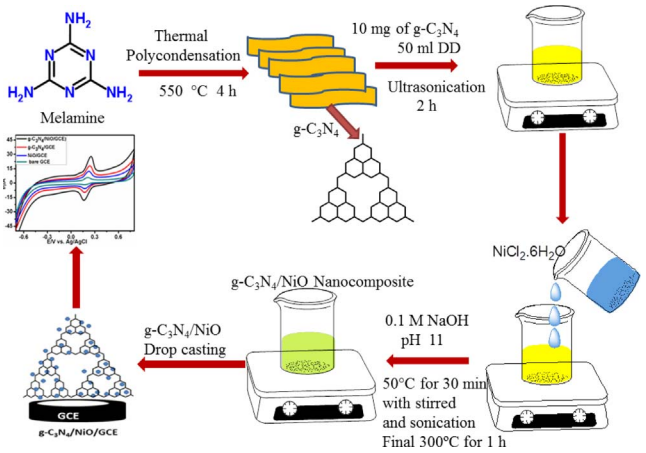

Scheme 2. Stepwise fabrication of g-C_3N_4/NiO modified glassy carbon electrode for QR sensor.

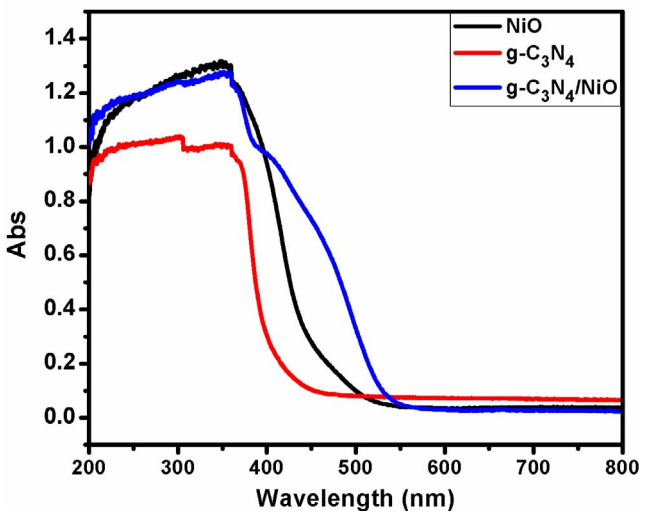

Fig. 1. Optical properties of g-C_3N_4, NiO and g-C_3N_4/ NiO nanocomposite.

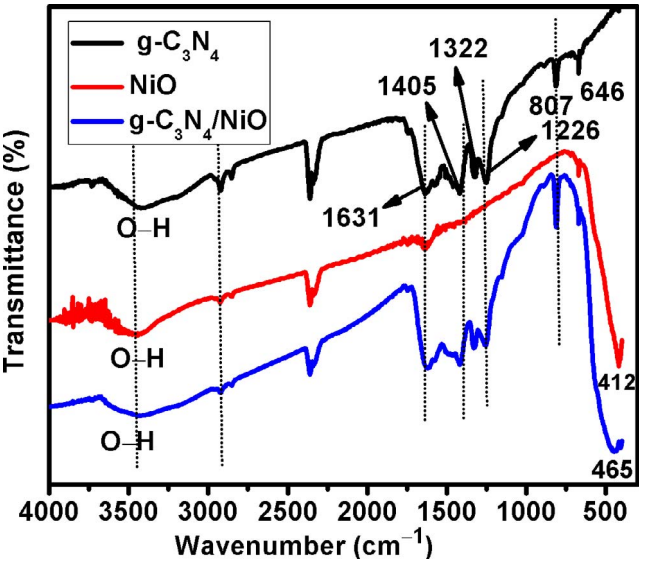

Fig. 2. FT-IR spectra of g-C_3N_4, NiO and g-C_3N_4/NiO nanocomposite.

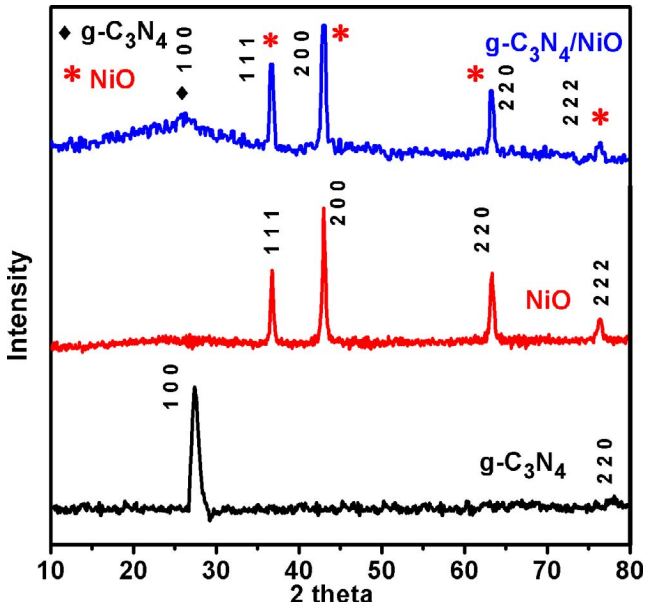

Fig. 3. XRD pattern of g-C_3N_4, NiO and g-C_3N_4/NiO nanocomposite.

2.5. Instruments

Electrochemical measurements were performed with a computer-controlled electrochemical workstation (CH-660E Instruments Texs USA) and a computer-controlled advanced electrochemical system in a two-compartment electrochemical cell with a bare or modified GCE (3 mm in diameter) working electrode, a platinum wire counter electrode, and an (Ag/AgCl)/ vs (KCl-saturated) reference electrode. All of the electrochemistry experiments were performed at room temperature. The surface morphological characterization of g-C_3N_4/NiO/GCE was examined by means of scanning electron microcopy (SEM; JEOL JSM 6701F) at an accelerating voltage of 20 kV. The crystalline structure of the nanoparticles was studied by an X-ray diffraction (XRD; XPERT PRO X-RAY) with Cu Kα radiation at 25 °C and the structural assignments were made with reference to the JCPDS power diffraction files. Fourier transform infrared (FT-IR) measurements were performed using a Perkin Elmer spectrophotometer RXI. Hitachi U-3300 spectrophotometer was used to carry out UV–visible absorption spectroscopy measurements.

3. Results and discussions

3.1. Optical properties

The optical properties of the prepared nanocomposite are very essential factor for determining their electrocatalytic efficiency. Fig. 1 shows the UV–vis-spectra of absorption onset observed at about 380 nm for g-C_3N_4, 330 nm for NiO and 410 nm for g-C_3N_4/NiO [43]. It can be seen from the figure that the absorbance intensity of g-C_3N_4/NiO nanocomposite was shifted to a longer wavelength when compared to g-C_3N_4 and NiO. The observed red shift in g-C_3N_4/NiO nanocomposite can be attributed to the electron–hole transition between g-C_3N_4 and NiO. The above result indicates that dispersing NiO on the g-C_3N_4 surface leads to the enhanced absorption in the visible light range, which is an important tool for the electrocatalytic application.

3.2. FT-IR

The molecular structure information of the as prepared samples g-C_3N_4, NiO and g-C_3N_4/NiO nanocomposite, as depicted in Fig. 2. With respect to g-C_3N_4 (block line), the prominent bands in the region of

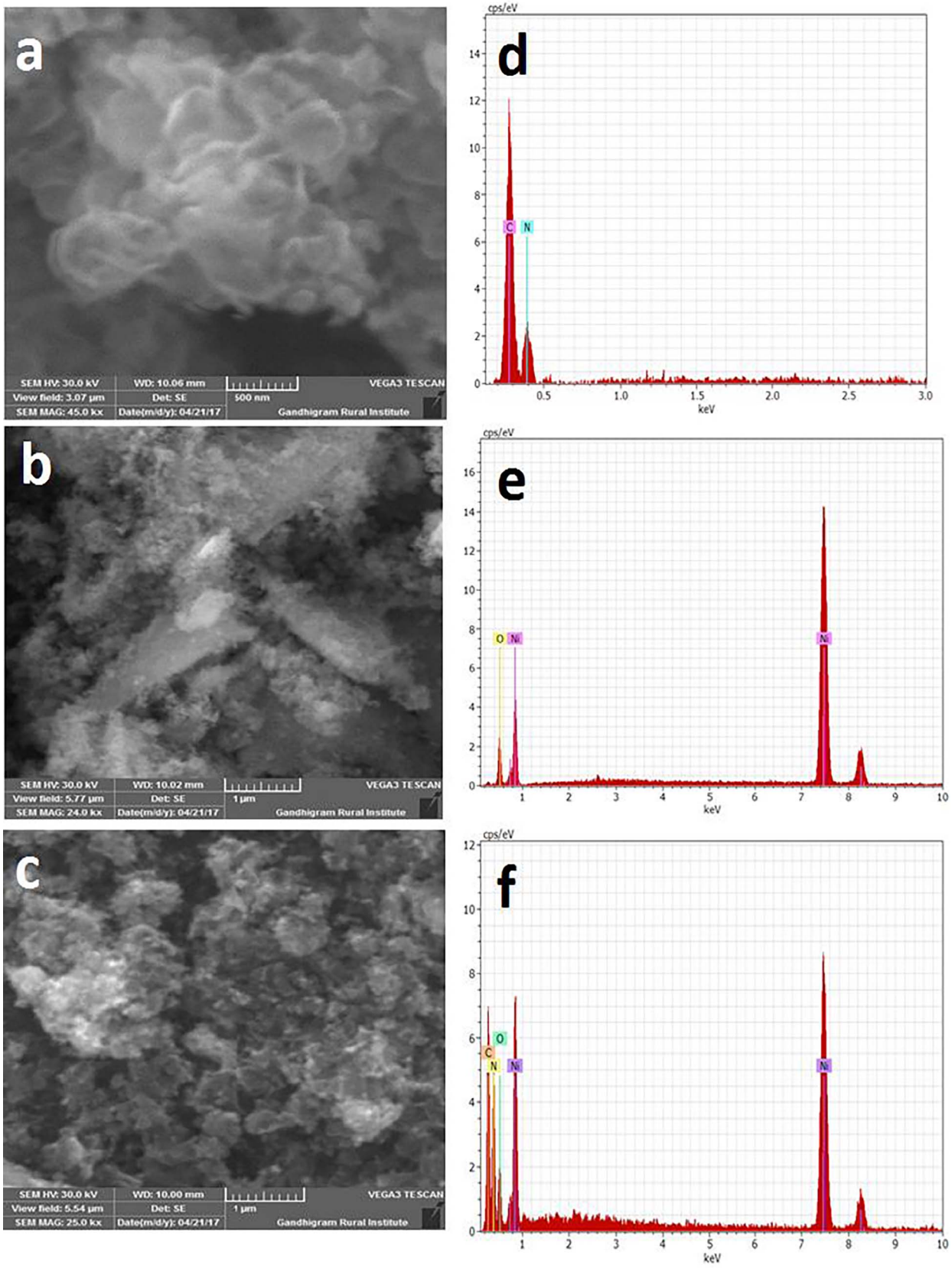

Fig. 4. SEM image of (a) g-C_3N_4, (b) NiO and (c) g-C_3N_4/NiO nanocomposite.

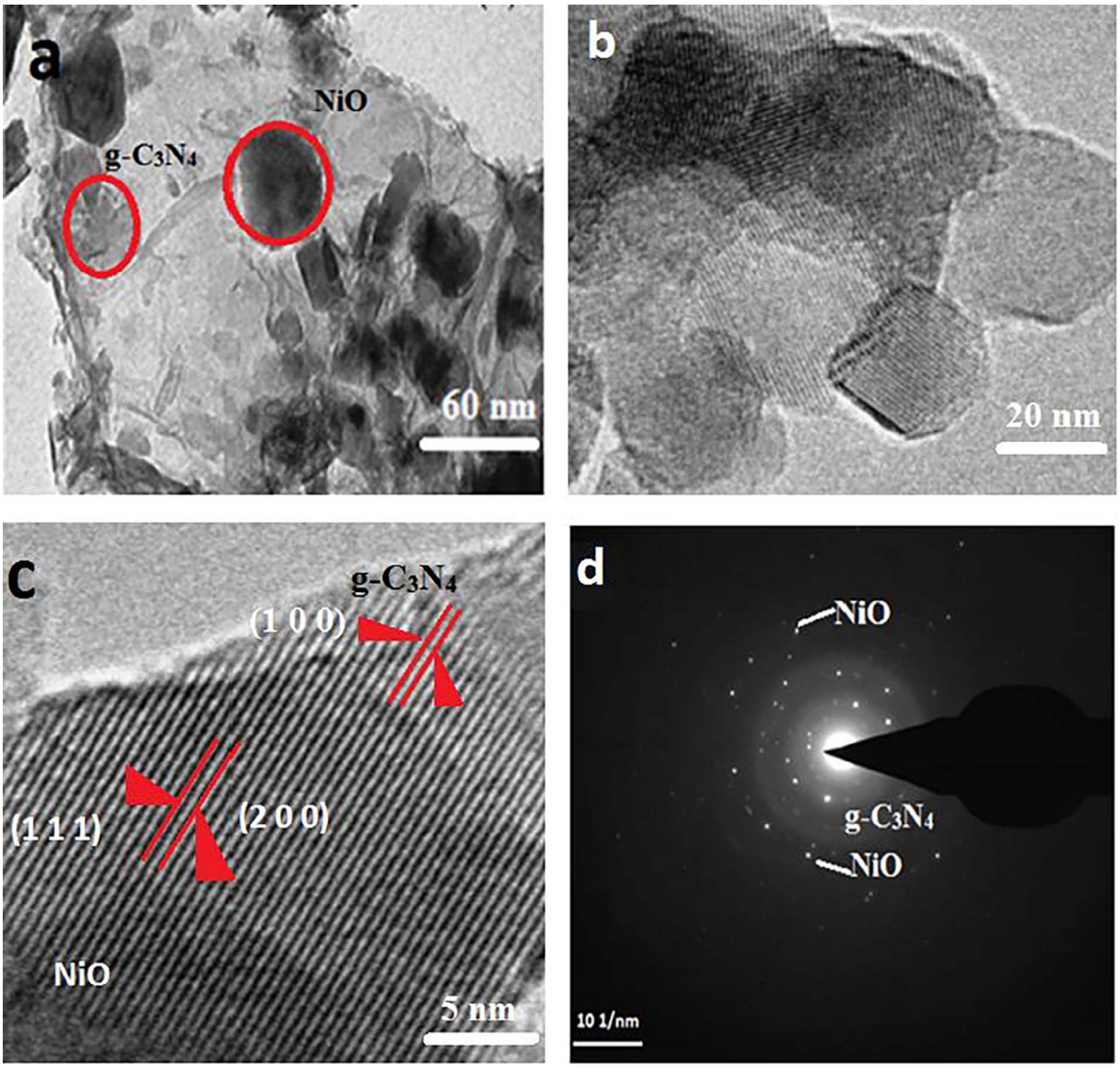

Fig. 5. HRTEM image of g-C_3N_4/NiO nanocomposite with SAED pattern.

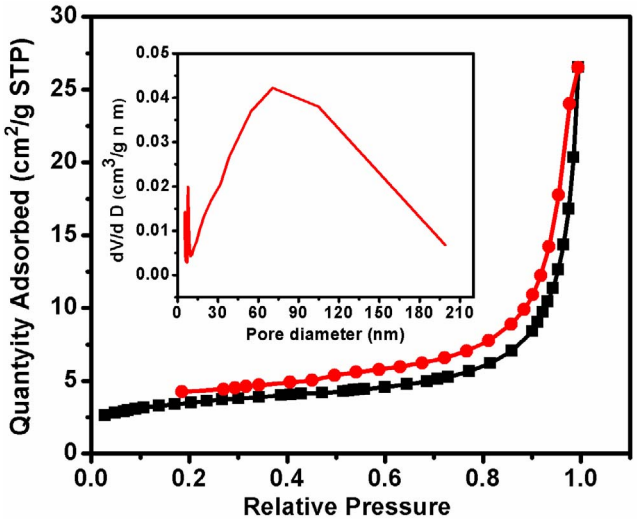

Fig. 6. Nitrogen adsorption-desorption isotherm and corresponding pore size distribution curve (inset) of the g-C_3N_4/NiO nanocomposite.

1200–1650 cm^{-1} can be related to the typical stretching modes of CN heterocycles, wherein the peaks at 1226, 1322, 1405, 1631 cm^{-1} are assigned to the aromatic C—N stretching. The sharp band sat 807 cm^{-1}, 646 cm^{-1} are attributed to the bending vibration of characteristics of triazine rings [47,48]. The broad peaks at around 2900–3400 cm^{-1} originate from stretching vibration modes for the –NH and hydroxyl of the adsorbed H_2O. The broad absorption bands at around 412 cm^{-1}, 698 cm^{-1} and 1652 cm^{-1} are attributed to the Ni–O (red line) vibration absorption [49], while the broad absorption region with a maximum around 3632 cm^{-1} can be attributed to the hydroxyl groups and adsorbed water [49]. The peak observed at 412 cm^{-1} of NiO is shifted to 465 cm^{-1} in the case of nanocomposite. These results suggest that the hydroxyl groups and triazine rings of g-C_3N_4 are successfully interact with NiO via hydrogen bonding or electrostatic interaction.

3.3. X-ray diffraction

The phase and composition of as prepared samples of g-C_3N_4, NiO and g-C_3N_4/NiO nanocomposite were investigated by powder X-ray diffraction pattern and are displayed in Fig. 3. The XRD pattern of the g-C_3N_4 show two obvious peaks at 27.45°, which correspond to the (1 0 0) and (0 0 2) planes of g-C_3N_4, consistent with the standard value (JCPDS

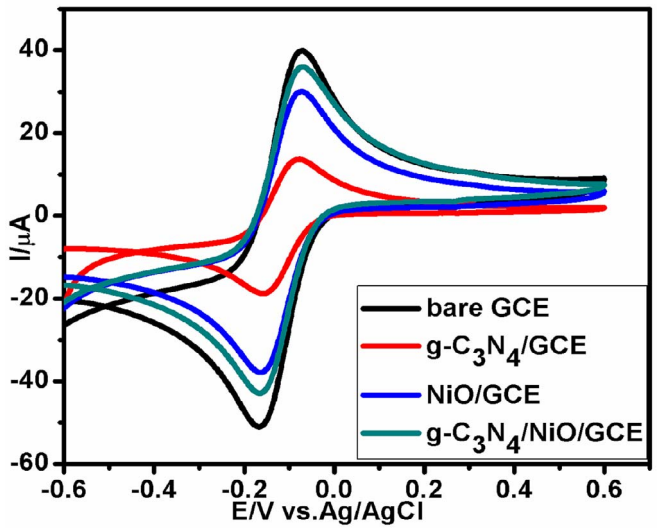

Fig. 7. CV of bare GCE, g-C_3N_4/GCE, NiO/GCE, and g-C_3N_4/NiO/GCE in phosphate buffer saline (0.1 M PBS, pH, 6.4) containing 5 mM $[Fe(CN)_6]^{3-/4-}$ at scan rate of 50 mV/s.

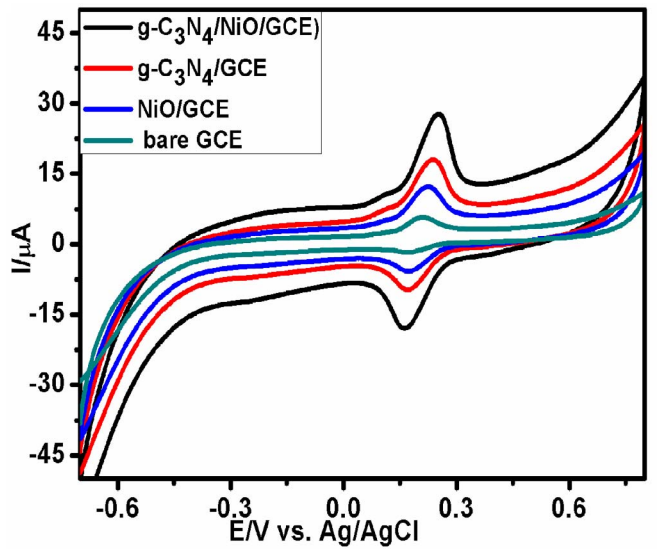

Fig. 8. CVs of 5 μM QR on the bare GCE, NiO/GCE (b), g-C_3N_4/GCE (c) and g-C_3N_4/NiO/GCE in 0.1 M PBS (pH 6.4) at scan rate of 50 mV/s.

87-1526). The XRD pattern of the pure NiO demonstrates sharp diffraction peaks at 37.26°, 43.26°, 62.81°, and 79.36°, which can be respectively indexed to the crystal planes of (111), (200), (220) and (222) of pure NiO nanoparticles (Cubic structure, JCPDS 47-1049). The g-C_3N_4/NiO nanocomposite peaks located at 27.32°, 38.01°, 44.23°, 64.31°, and 76.35° corresponding to (100), (111), (200), (220) and (222) respectively. The FT-IR result shows good coincidence with XRD analysis and indicates the hybrids structure of g-C_3N_4/NiO nanocomposite. The average crystallite sizes are calculated from Debye-Scherrer equation [50].

3.4. Surface morphology and microstructure

The SEM images of g-C_3N_4, NiO and g-C_3N_4/NiO nanocomposite are illustrated in Fig. 4(a–c). As seen from the figure, g-C_3N_4 nanoparticles have sheet-like structure, NiO nanoparticles are spherical like in shape and the g-C_3N_4/NiO nanocomposite has short sphere like morphology in the average range 30–60 nm. The dark grey spheres in the micrographs are obviously NiO and g-C_3N_4 has white small pinches on the grey surface of NiO. The EDX spectrum and their corresponding keV of g-C_3N_4, NiO and g-C_3N_4/NiO nanocomposite are displayed in Fig. 4d–f. The peaks corresponding to C, N Ni and O are clearly observed in the EDX spectrum at their normal energy and the results are clearly indicating the formation of g-C_3N_4/NiO nanocomposite.

The surface morphology and particle size of g-C_3N_4/NiO nanocomposite was further verified by different magnification of HR-TEM (Fig. 5a–c), which showed direct information about the distribution of the g-C_3N_4 on the nanocomposite surface. TEM observation reveals that there are no discrete NiO or g-C_3N_4 nanoparticles. The bright grey and black color spherical agglomerates are obviously due to the presence of g-C_3N_4 and NiO, which is beneficial for the formation of g-C_3N_4/NiO nanocomposite SAED (selected area electron diffraction) as shown Fig. 5d. The average particle size was found to be 60–5 nm, which is in good agreement with the XRD results [50].

3.5. BET

In order to investigate the mesoporous nature and specific surface area of the as-synthesized g-C_3N_4/NiO composite, a nitrogen adsorption – desorption isotherm was successfully measured at −195.87 °C. The isotherm for the sample, which exhibits a type IV with a H_3 hysteresis loop according to the IUPAC classification, reflecting the presence of a mesoporous structure of the composite is displayed in Fig. 6. The surface area ($S_{B.E.T.}$ (m^2/g)) of g-C_3N_4 and NiO has been calculated using B.E.T equation and it was found to be 86.51 m^2/g and 81.32 m^2/g. The pore-size distribution of the sample is also estimated using the Barrett–Joyner–Halenda (BJH) method from the desorption branch of the isotherm, as shown in the inset of Fig. 6. The calculated pore size distribution using BJH method indicates that the size of mesoporous is not uniform ranging from 10 to 80 nm, which is consistent with the HR-TEM observation [51].

3.6. Electrochemical studies

Fig. 7. shows CV of bare GCE, g-C_3N_4/GCE, NiO/GCE, and g-C_3N_4/NiO/GCE recorded in phosphate buffer saline (0.1 M PBS, pH, 6.4) containing 5 mM $[Fe(CN)_6]^{3-/4-}$ and in the potential range, −0.3 to 0.6 V at 50 mV/s rate. The bare GCE (curve a) shows a well-defined pair of redox peaks corresponding to the electrochemical behavior of $[Fe(CN)_6]^{3-/4-}$. When the g-C_3N_4 and NiO are individually applied on to the surface of GCE, a decrease in both oxidation and reduction peak current is noticed. Furthermore, the g-C_3N_4 coated onto the surface of NiO/GCE has increased both oxidation and reduction peak current. In the case g-C_3N_4/NO composite modified GCE has excellent electrochemical properties.

3.7. Electrochemical behavior of QR in g-C_3N_4/NiO/GCE

Fig. 8 displayed the electrochemical behavior of 5 μM QR on the bare GCE, NiO/GCE, g-C_3N_4/GCE and g-C_3N_4/NiO/GCE investigated by CV in 0.1 M PBS (pH 6.4) at a scan rate of 50 mV/s. In the case of bare GCE small redox peaks at E_{pa}0.216 V and E_{pc} 0.158 V are observed where as the current increased after g-$C_3N_4$was deposited onto GCE, which was ascribed to the g-C_3N_4 impeding the transfer of electrons. It also demonstrated that g-$C_3N_4$was successfully modified to the electrode. However, when g-C_3N_4 is applied onto the surface of NiO/GCE, the oxidation current of QR was dramatically increased due to the excellent synergetic effect of g-C_3N_4/NiO/GCE.

To investigate the electron transfer rate of the g-C_3N_4/NiO/GCE, the CV response of QR at different scan rate (10–100 mV) are displayed in Fig. 9a. In the case of anodic and cathodic peak currents increased linearly with the scan rate are increases. As shown Fig. 9b, the relationship between oxidation peak current, reduction peak current and the square root of the scan can be expressed as: I_{pa} = 0.6791x + 26.0709c with a correlation coefficient (R^2) = 0.9902

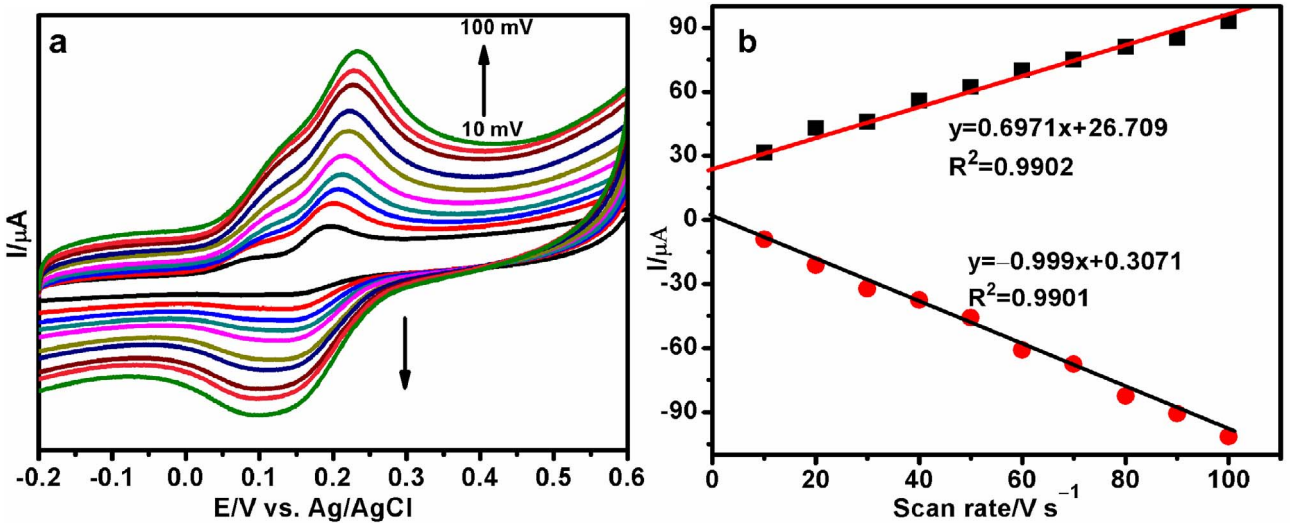

Fig. 9. (a) CVs of 10 μM QR on the g-C_3N_4/NiO/GCE at different scan rate 10–100 mV/s in 0.1 M PBS. (b) The relationship between the redox peak potential and the Napierian logarithm of scan rate.

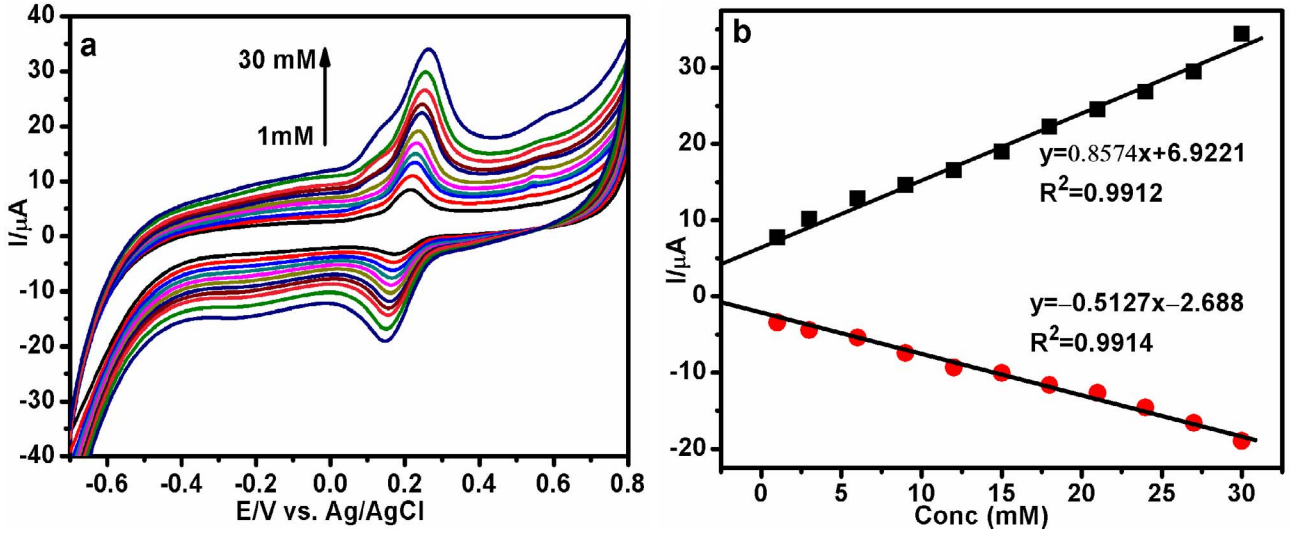

Fig. 10. (a) CVs of varying QR concentration in the range of 1–30 mM in 0.1 M PBS (pH 6.4). (b) Inset: calibration plot in concentration vs current.

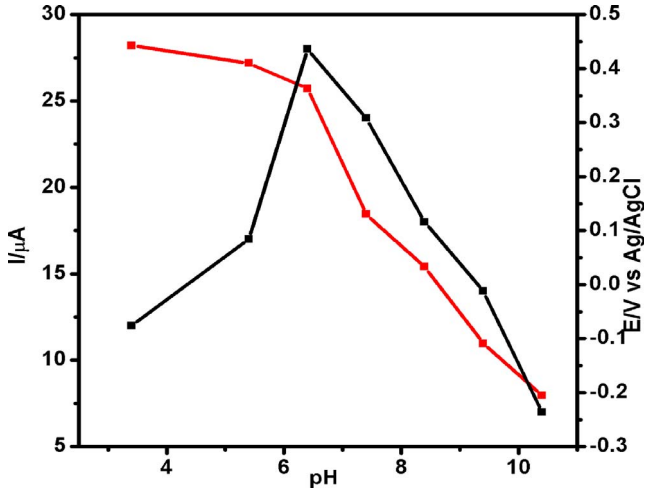

Fig. 11. Effect of pH.

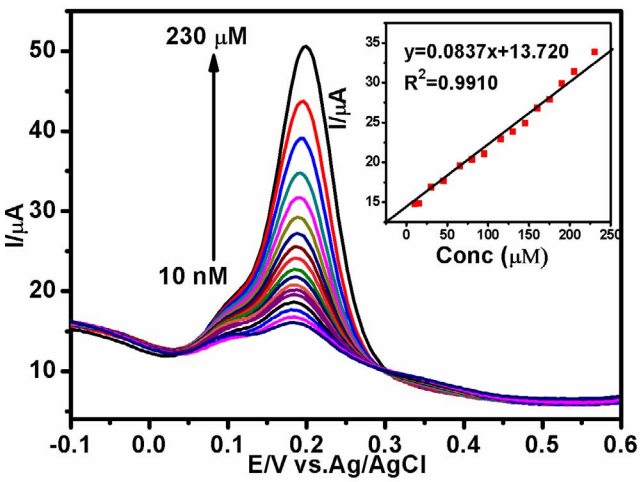

Fig. 12. DPV of the g-C_3N_4/NiO/GCE in 0.1 M PBS (pH = 6.4) for different concentrations of QR.

Table 1
Comparison of analytical performance of QR sensing by various modified electrode.

Electrode	Linear range (μM)	Detection Limit (μM)	Method	Stability	Refs.
Bare GCE	0.1–15	0.0031	DPV	–	[52]
DNA/CPE	0.1–3	0.0385	DPV	–	[53]
CPE/AM	0.025–1.5	0.010	DPV	–	[26]
E-Gr/P-β-CD/GCE	0.005–20	0.001	DPV	2 weeks	[54]
GCE/PEI-CNTs	0.8–7.0	0.89	SWV	–	[55]
GCE/PAA–CNTs	0.1–5.0	0.0075	Amperometric	–	[55]
GOD/AuNP/GCE	0.01–6.0	0.002	DPV	1 week	[56]
Co_3O_4/GCE	0.050 –33	100 nM	DPV	4 week	[57]
g-C_3N_4/NiO/GCE	0.010–230	0.002	DPV	4 weeks	This work

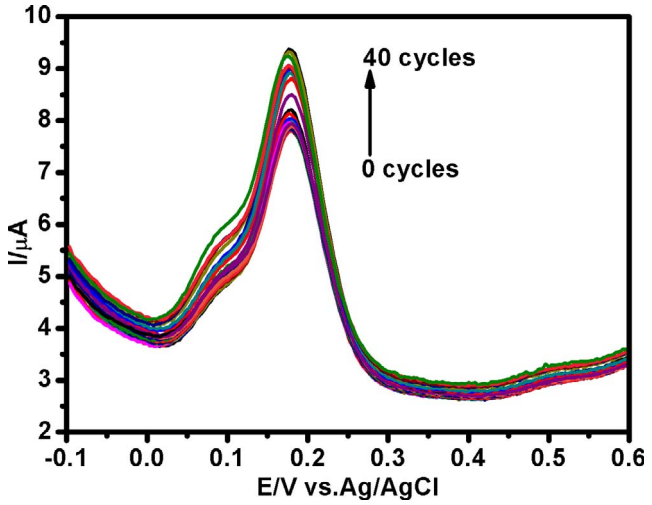

Fig. 13. Differential pulse voltammograms for 40 multiple cycles in the presence 10 μM QR at g-C_3N_4/NiO/GCE in 0.1 M PBS (pH6.4).

Table 2
Determination QR in green tea, green apple and honeysuckle.

Sample	Detected	Added	Found	Recovery	RSD (n = 3)
Green Tea	6.67 ± 21	6	12.45	99.00	2.122
Green Apple	7.12 ± 34	6	13.54	101.56	3.163
Honeysuckle	6.87 ± 54	6	12.56	101.94	2.125

and $I_{pc} = -0.999x + 0.3071$ with a correlation coefficient (R^2) = 0.9901, respectively.

The effect of the QR concentration on the CV response for the g-C_3N_4/NiO/GC electrode was also investigated, and the results are shown in Fig. 10a. It can be seen that the gradual addition of QR causes an increase in the oxidation current, and this increase was found to be linear (Fig. 10b). These observations further suggest that the g-C_3N_4/NiO nanocomposite displays a good response towards the oxidation of QR. This result shows better catalytic properties than those of *ortho*-quinone.

Further, QR is a phenolic aromatic compound and its existing form is strongly dependent on the pH of the aqueous, which influenced its redox process on the electrode; on the other hand, the electrochemical oxidation of QR on the modified electrode surface is a procedure with the proton participation. These two aspects both were relative to the pH, so, the effect of pH on the electrochemical response of QR was investigated. To achieve an optimal electrochemical response of 0.1 M PBS containing 10 μM QR at g-C_3N_4/NiO/GCE, the effect of pH vs current and potential were investigated by CV in the range of 3.8–7.6. As can be seen in Fig. 11, the redox peak current increased with solution pH ranging from 3.8 to 6.4, and then the decrease of the redox peak current was observed when the solution pH was higher than 6.4. Therefore, the influence of pH value of 6.4 was chosen as the optimal pH condition and utilized in the subsequent experiments. Meanwhile, the oxidation peak potentials shifted negatively with the increase of pH value, which is due to the anodic reaction which is much easier under pH 6.4. The values of oxidation peak potential shifted to more negative potentials with the increase of pH indicating that protons take part in the electrode reaction process.

DPV was used for the determination of QR because of its higher sensitivity than CV. Further, DPV was performed to examine the sensitivity of the g-C_3N_4/NiO/GCE towards the detection of QR. Fig. 12 displayed the DPV of the g-C_3N_4/NiO/GCE in 0.1 M PBS (pH = 6.4) for different concentrations of QR. Here the DPV was recorded by sweeping the potential between −1.0 and 0.6 V at amplitude of 0.05 V, a step potential of 0.07 V and a scan rate of 20 mV s^{-1}. In case of DPV, curve a–j show the well-defined and stable anodic oxidation peak current curves for QR. These results demonstrated that the g-C_3N_4/NiO/GCE might provide a good electrocatalytic activity towards QR sensing. The DPVs current linearly increased when the concentration of QR was increased from 0.01 μM to 250 μM at g-C_3N_4/NiO/GCE with a correlation coefficient of 0.9910 (inset Fig. 8) and detection limit is 0.002 μM. Linear range and detection limit are compared with reported data summarized in Table 1. The present electrochemical sensor showed on excellent electrochemical detection of QR.

3.8. Study of interference, repeatability, reproducibility and real samples

Some organic compounds and inorganic ions were tested to check their levels of interference in QR determination. The selectivity and utility of the proposed method were investigated in the presence of coexisting ions. For this purpose, the interference of various ions was tested in optimized conditions by adding them to the solution containing 10 μM QR. The tolerable limit was defined as the foreign ion concentration that gave an error of less than ± 3.0%. Experimental results showed there is no interference for ions with a 500-fold excess of Co^{2+}, Pb^{2+}, Ca^{2+},Na+, and Mg^{2+}, a 200-fold excess of Fe^{2+}, a 100-fold excess of Ni^{2+}, and a 10-fold excess of Cd^{2+}, Cu^{2+}.

The reproducibility and stability of the sensor were evaluated in the presence of 10 mM QR. The relative standard deviation (RSD) was calculated to be 1.3% by repeated detection of the catalytic currents for 40 times (Fig. 13) on the same electrode. Similarly, the RSD was 1.3% for five electrodes constructed independently. Additionally, the storage stability of the modified electrode was checked after the one-month storage at 25 °C, the catalytic currents retained 95.64% of the initial value. These phenomena demonstrate the improved reproducibility and stability of the resulting sensor.

The g-C_3N_4/NiO/GCE for the real samples determination was performed by measuring green tea, green apple and honeysuckle sing the standard addition technique. All samples were diluted with 0.1 M PBS (pH = 6.4) and transferred to the electrochemical cell before the measurements. In order to ascertain the correctness of the results, certain amounts of green apple, honeysuckle, and green tea were added into the diluted samples and then detected. The results were summarized in Table 2. One can see that g-C_3N_4/NiO/GCE exhibited exact recovery results, which indicated that RGO/GCE has the potential application for determining QR in real samples.

4. Conclusion

In summary, g-C_3N_4/NiO nanocomposite modified GCE for the ultra-sensitive determination of QR. The UV–vis, FT-IR, XRD, SEM with EDX, HRTEM, and B.E.T techniques suggested the existence of strong interfacial interaction between g-C_3N_4 and NiO. DPV current has a wide

linear dynamic range 10 nM to 250 μM and limit of detection was found to be (LOD) 0.002 μM. This implies the excellent electrochemical sensing nature of the fabricated g-C_3N_4/NiO composites sensor over reported literature with good sensitivity and selectivity. The sensor doesn't exhibit any remarkable change in the presence of interferents. The proposed sensor also showed good stability, repeatability and reproducibility. The fabricated electrochemical sensor was further intended for the detections of QR in various real samples like green apple, green tea and honeysuckle. Thus, g-C_3N_4 / NiO nanocomposite can hopefully be applied to other research fields due to its unique electrochemical properties.

Acknowledgements

The authors are grateful to DST-SERB (SB/S1/IC-06/2013 dt:03/09/2014) India for providing financial support. The management of Thiagarajar College is acknowledged for providing necessary laboratory facilities.

References

[1] S.B. Nimse, D. Pal, Free radicals, natural antioxidants, and their reaction mechanisms, RSC Adv. 5 (2015) 27986–28006.
[2] Q. Duan, J. Cao, J. Zhang, Analysis of phenolic acids and their antioxidant activity by capillary electrophoresis-mass spectrometry with field-amplified sample injection, Anal. Methods 4 (2012) 3027–3032.
[3] B. Tu, Z.-J. Liu, Z.-F. Chen, Y. Ouyang, Y.-J. Hu, Understanding the structure–-activity relationship between quercetin and naringenin: in vitro, RSC Adv. 5 (2015) 106171–106181.
[4] S. Das, U. Rayachaudhuri, M. Falchi, A. Bertelli, P.C. Braga, D.K. Das, Cardioprotective properties of raw and cooked eggplant (Solanum melongena L.), Food Funct. 2 (2011) 395–399.
[5] B. Badhani, N. Sharma, R. Kakkar, Gallic acid: a versatile antioxidant with promising therapeutic and industrial applications, RSC Adv. 5 (2015) 27540–27557.
[6] S. Sen, R. Chakraborty, The role of antioxidants in human health, ACS Symp. Ser. 1083 (2011) 1–37.
[7] Y. Yao, J. Liu, W. Liu, M. Zhao, B. Wu, J. Gu, Z. Zou, Vitamin E assisted polymer electrolyte fuel cells, Energy Environ. Sci. 7 (2014) 3362–3370.
[8] M.J. Thomas, The role of free radicals and antioxidants, M. J. Nutr. 16 (2000) 716–718.
[9] V. Lobo, A. Patil, A. Phatak, N. Chandra, Free radicals, antioxidants and functional foods: impact on human health, Pharmacogn. Rev. 4 (2010) 118–126.
[10] E. Niki, Antioxidant capacity of foods for scavenging reactive oxidants and inhibition of plasma lipid oxidation induced by multiple oxidants, Food Funct. 7 (2016) 2156–2168.
[11] P. Ferri, D. Angelino, L. Gennari, S. Benedetti, P. Ambrogini, P.D. Grande, P. Ninfali, Enhancement of flavonoid ability to cross the blood–brain barrier of rats by co administration with α-tocopherol, Food Funct. 6 (2015) 394–400.
[12] M.M. Kasprzak, A. Erxleben, J. Ochocki, Properties and applications of flavonoid metal complexes, RSC Adv. 5 (2015) 45853–45877.
[13] S.A. Mohamed, M.A. Awad, E.-R.F.A. El-Dengawy, H.M. Abdel Mageed, M.O. El Badry, H.A. Salah, A.M. Abdel-Aty, A.S. Fahmy, Total phenolic and flavonoid contents and antioxidant activities of sixteen commercial date cultivars grown in Saudi Arabia, RSC Adv. 6 (2016) 44814–44819.
[14] P. Li, J. Jia, D. Zhang, J. Xie, X. Xu, D. Wei, In vitro and in vivo antioxidant activities *of a* flavonoid isolated from celery (*Apiumgraveolens* L. var. dulce), Food Funct. 5 (2014) 50–56.
[15] L.M. Berger, S. Wein, R. Blank, C.C. Metges, S. Wolffram, Bioavailability of the flavonol quercetin in cows after intraruminal application of quercetin aglycone and rutin, J. Dairy Sci. 95 (2012) 5047–5055.
[16] R.T. Johnson, C.E. Lunte, A capillary electrophoresis electrospray ionization-mass spectrometry method using a borate background electrolyte for the fingerprinting analysis of flavonoids in Ginkgo biloba herbal supplements, Anal. Methods 8 (2016) 3325–3332.
[17] H. Zhang, M. Kang, H. Zhang, Y. Yu, Matrix solid phase dispersion extraction for determination of flavonoids in the flower of chrysanthemum morifolium Ramat. By capillary zone electrophoresis, RSC Anal. Methods 6 (2014) 766–773.
[18] Y. Pang, Y.-K. Huang, F. Li, F.-Q. Yang, Z.-N. Xia, Rapid screening and evaluation of antioxidants in alkaloid natural products by capillary electrophoresis with chemiluminescence detection, Anal. Methods 8 (2016) 6545–6553.
[19] L.R. Tallini, G.P.R. Pedrazza, S.A.L. Bordignon, A.C.O. Costa, M. Steppe, A. Fuentefria, J.A.S. Zuanazzi, Analysis of flavonoids in rubusery throcladus and morus nigraleaves extracts by liquid chromatography and capillary electrophoresis, Rev. Bras. Farmacognosia 25 (2015) 219–227.
[20] S.G. Dmitrienko, V.A. Kudrinskaya, V.V. Apyari, Methods of extraction, preconcentration, and determination of quercetin, J. Anal. Chem. 67 (2012) 299–311.
[21] L.A.L. Silva, B.R. Pezzini, L. Soares, Spectrophotometric determination of the total flavonoid content in ocimumbasilicum L. (Lamiaceae) leaves, Pharmacogn. Mag. 11 (2015) 96–101.
[22] H. Xu, Y. Li, H.-W. Tang, C.-M. Liu, Q.-S. Wu, Determination of rutin with UV–Vis spectrophotometric and laser-induced fluorimetric detections using a non-scanning spectrometer, Anal. Lett. 43 (2010) 893–904.
[23] M.T. Falkova, M.O. Pushina, A.V. Bulatov, G.M. Alekseeva, L.N. Moskvin, Stepwise injection spectrophotometric determination of flavonoids in medicinal plants, Anal. Lett. 47 (2014) 970–982.
[24] A. Masek, M. Zaborski, E. Chrzescijanska, Electrooxidation of flavonoids at platinum electrode studied by cyclic voltammetry, Food Chem. 127 (2011) 699–704.
[25] A. Masek, E. Chrzescijanska, M. Zaborski, Electrooxidation of morin hydrate at a Pt electrode studied by cyclic voltammetry, Food Chem. 148 (2014) 18–23.
[26] Y. Li, W. Huang, Electrode modified with porous alumina microfibers as a highly sensitive electrochemical sensor for quercetin, Anal. Methods 7 (2015) 2537–2541.
[27] Y.-Y. Yao, L. Zhang, Z.-F. Wang, J.-K. Xu, Y.-P. Wen, Electrochemical determination of quercetin by self-assembled platinu nanoparticles/poly (hydroxy methylated-3,4-ethylene dioxylthiophene) nanocomposite modified glassy carbon electrode, Chin. Chem. Lett. 25 (2014) 505–510.
[28] S. Sun, M. Zhang, Y. Li, X. He, A molecularly imprinted polymer with incorporated graphene oxide for electrochemical determination of quercetin, Sensors 13 (2013) 5493–5506.
[29] Z. Zhang, S. Gu, Y. Ding, M. Shen, L. Jiang, Mild and novel electrochemical preparation of β-cyclodextrin/graphene nanocomposite film for super-sensitive sensing of quercetin, Biosens. Bioelectron. 57 (2014) 239–244.
[30] A. Moghtada, R. Ashiri, Superiority of sonochemical processing method for the synthesis of barium titanate nanocrystals in contrast to the mechanochemical approach, Ultrason. Sonochem. 41 (2018) 127–133.
[31] A. Moghtada, R. Ashiri, Nanocrystals of $XTiO_3$ (X = Ba, Sr, Ni, BaxTi1 − x) materials obtained through a rapid one-step methodology at 50 °C, Ultrason. Sonochem. 26 (2015) 293–304.
[32] A. Moghtada, R. Ashiri, Carbonate-free strontium titanium oxide nanosized crystals with tailored morphology: facile synthesis, characterization, and formation mechanism, Metall. Mater. Trans. B 45 (2014) 1979–1986.
[33] P. Si, Y. Huang, T. Wang, J. Ma, Nanomaterials for electrochemical non-enzymatic glucose biosensors, RSC Adv. 3 (2013) 3487–3502.
[34] N. Pokhrel, P.K. Vabbina, N. Pala, Sonochemistry: science and engineering, Ultrason. Sonochem. 29 (2016) 104–128.
[35] X.D. Zhang, X. Xie, H. Wang, J.J. Zhang, B.C. Pan, Y. Xie, Enhanced photoresponsive ultrathin graphitic-phase C_3N_4 nanosheets for bioimaging, J. Am. Chem. Soc. 135 (2013) 18–21.
[36] M. Amiri, H. Salehniya, A.H. Yangjeh, Graphitic carbon nitride/chitosan composite for adsorption and electrochemical determination of mercury in real samples, Ind. Eng. Chem. Res. 55 (2016) 8114–8122.
[37] J. Zhang, Z. Zhu, J. Di, Y. Long, W. Li, Y. Tu, A sensitive sensor for trace Hg^2 determination based on ultrathin g-C_3N_4 modified glassy carbon electrode, Electrochim. Acta 186 (2015) 192–200.
[38] L. Xu, J.X. Xia, H. Xu, S. Yin, K. Wang, L.Y. Huang, L.G. Wang, H.M. Li, Reactable ioniliquid assisted solvothermal synthesis of graphite-like C_3N_4 hybridized α-Fe_2O_3 hollow microspheres with enhanced supercapacitive performance, J. Power Sources 245 (2014) 866–874.
[39] A. Majeed, W. Ullah, A.W. Anwar, F. Nasreen, A. Sharif, G. Mustafa, A. Khan, Graphen metal oxides/hydroxide nanocomposite materials: fabrication advancements and supercapacitive performance, J. Alloys Compd. 671 (2016) 1–10.
[40] N.S.K. Gowthaman, S. Abraham John, Modification of a glassy carbon electrode with gold platinum core–shell nanoparticles by electroless deposition and their electrocatalytic activity, RSC Adv. 5 (2015) 42369–42375.
[41] V. Balakumar, P. Prakash, A facile *in-situ* synthesis of highly active and reusable ternary Ag-PPy-GO nanocomposite for catalytic oxidation of hydroquinone in aqueous solution, J. Catal. 344 (2016) 795–805.
[42] L. Ye, D. Wang, S. Chen, Fabrication and enhanced photoelectrochemical performance of MoS_2/S-doped g-C_3N_4 heterojunction film, ACS Appl. Mater. Interfaces 8 (2016) 5280–5289.
[43] B. Hu, F. Cai, T. Chen, M. Fan, C. Song, X. Yan, W. Shi, Hydrothermal synthesis g-C_3N_4/Nano-$InVO_4$ nanocomposites and enhanced photocatalytic activity for hydrogen production under visible light Irradiation, ACS Appl. Mater. Interfaces 7 (2015) 18247–18256.
[44] N.S.K. Gowthaman, M. Amal Raj, S. Abraham John, Nitrogen-doped graphene as a robust scaffold for the homogeneous deposition of copper nanostructures: a non enzymatic disposable glucose sensor, ACS Sustainable Chem. Eng. 5 (2017) 1648–1658.
[45] A. Baishnisha, P. Selvakumar, Shen-Ming Chen, V. Velusamy, Te-Wei Chiu, Tse-Wei Chen, R. SayeeKannan, A non-enzymatic amperometric hydrogen peroxide sensor based on iron nanoparticles decorated reduced graphene oxide nanocomposite, J. Colloids Interface. Sci. 487 (2017) 370–377.
[46] L. Li, Y. Hu, D. Deng, H. Song, Y. Lv, Highly sensitive cataluminescence gas sensors for 2-butanone based on g-C_3N_4 sheets decorated with CuO nanoparticles, Anal. Bioanal. Chem. 408 (2016) 8831–8841.
[47] F.-T. Li, Y. Zhao, Q. Wang, X.-J. Wang, Y.-J. Hao, R.-H. Liu, Enhanced visible-light photocatalytic activity of active Al_2O_3/g-C_3N_4 heterojunctions synthesized via surface hydroxyl modification, J. Hazard. Mater. 283 (2015) 371–381.
[48] B. Vellaichamy, P. Periakaruppan, Catalytic hydrogenation performance of an in situ assembled Au@g-C_3N_4–PANI nanoblend: synergistic inter-constituent interactions boost the catalysis, New J. Chem. 41 (2017) 7123–7132.
[49] M. El-Kemary, N. Nagy, I. El-Mehasseb, Nickel oxide nanoparticles: synthesis and spectral studies of interactions with glucose, Mater. Sci. Semi. Proc. 16 (2013) 1747–1752.
[50] S. Selvarajan, A. Suganthi, M. Rajarajan, K. Arunprasath, Highly efficient $BiVO_4$/WO_3 nanocomposite towards superior photocatalytic performance, Power Technol.

307 (2017) 203–212.
[51] J. Lv, K. Dai, J. Zhang, Q. Liu, C. Liang, G. Zhu, Facile constructing novel 2D porous g-C_3N_4/BiOBr hybrid with enhanced visible-light-driven photocatalytic activity, Sep. Purif. Technol. 178 (2017) 6–17.
[52] J. Yu, H. Jin, R. Gui, W. Lv, Z. Wang, A facile strategy for ratiometric electrochemical sensing of quercetin in electrolyte solution directly using bare glassy carbon electrode, J. Electroanal. Chem. 795 (2017) 97–102.
[53] A.K. Satpati, S. Sahoo, M.K. Dey, A.V.R. Reddy, T. Mukherjee, Electrochemical and spectroelectrochemical investigations of quercetin on unmodified and DNA-modified carbon paste electrode and its determination using voltammetry, Anal. Methods 3 (2011) 1344–1350.
[54] Z. Zhang, S. Gu, Y. Ding, M. Shen, L. Jiang, Mild and novel electrochemical preparation of β-cyclodextrin/graphene nanocomposite film for super-sensitive sensing of quercetin, Biosens. Bioelectron. 57 (2014) 239–244.
[55] F. Gutierrez, G. Ortega, J.L. Cabrera, M.D. Rubianes, G.A. Rivas, Quantification of quercetin using glassy carbon electrodes modified with multiwalled carbon nanotubes dispersed in polyethylenimine and polyacrylic acid, Electroanalsis 22 (2010) 2650–2657.
[56] J. Li, J. Qu, R. Yang, L. Qu, Peter de B. Harrington, A sensitive and selective electrochemical sensor based on graphene quantum dot/gold nanoparticle nanocomposite modified electrode for the determination of quercetin in biological samples, Electroanalysis 28 (2016) 1–10.
[57] M. Wang D. Zhang Z. Tong X. Xu X. Yang Voltammetric behavior and the determination of quercetin at a flowerlike Co3O4 nanoparticles modified glassy carbon electrode J. Appl. Electrochem. 41 2011 189 196.